Rev. Energ. Ren. Vol. 8 (2005) 1 - 18

Three-Dimensional Conjugate Conduction-Mixed Convection with Variable Fluid Properties in a Heated Horizontal Pipe

T. Boufendi and M. Afrid

Laboratoire de Physique Energétique, Faculté des Sciences,
Université Mentouri, Route de Aïn El-Bey, Constantine, Algérie

Abstract - *This study concerns the numerical simulation of the three dimensional conjugate conduction-mixed convection heat transfer in a horizontal heated pipe with a small wall thickness. The fluid physical properties are variable with temperature and the heat losses from the outer surface of the pipe to the ambient are considered. The model equations of continuity, momenta and energy are numerically solved with a finite volume method. The obtained results show that the thermal and the flow fields are three-dimensional, the non-uniformity of the heat flux at the interface wall-fluid is significant and the mean Nusselt number in the pipe is considerably increased. The numerical results of our study are in good agreement with those of an experimental work done with the same geometric, dynamic and thermal parameters.*

Résumé - *Cette étude concerne une simulation numérique tridimensionnelle d'un transfert thermique en convection mixte conjuguée à une conduction dans un conduit horizontal chauffé, dont la paroi est de faible épaisseur. Les propriétés physiques du fluide sont thermo dépendantes et les pertes thermiques entre la surface extérieure du conduit et le milieu ambiant sont considérées. Les équations modélisantes de continuité, du mouvement et de l'énergie sont numériquement résolues par la méthode des volumes finis. Les résultats obtenus montrent que les champs thermique et dynamique sont tridimensionnels, que la non-uniformité du flux thermique à l'interface paroi-fluide est significative et que le nombre de Nusselt moyen dans le tube augmente considérablement. Les résultats numériques de notre étude sont en bon accord avec ceux d'une étude expérimentale conduite avec les mêmes paramètres géométriques, dynamiques et thermiques.*

Keywords: Conjugate heat transfer - Mixed convection - Uninsulated horizontal - Pipe - Fluid flow - Variables properties.

1. INTRODUCTION

The heat transfer in heated pipes is a classical problem that is still an active area of research for different thermal application such as flat plat solar collectors, nuclear reactors and heat exchangers. The extensive theoretical and experimental research work on mixed convection are well grouped by Bergles [1, 2], Aung [3], Kakaç [4] and Polyakov [5]. The fundamental differences between the mixed and forced convections are well established. As an example of the studies concerning the mixed convection in pipes having a finite thickness we cite the experimental work of Morcos and Bergles [6]. They studied the fully developed mixed convection in circumferentially heated glass and steel pipes. This study shows that the fully developed mixed convection Nusselt number is larger than that of the fully developed forced convection (Nu = 4.364). Newell and Bergles [7] and Chen and Hwang [8] have consecutively correlated the mixed convection average Nusselt number by introduction of the wall conduction effect. The mentioned studies have shown the importance of the radial and circumferential heat conduction within the pipe solid thickness. The analytic study of Baughn [9] has shown that the azimuthal conduction is more important than the radial one for a small pipe thickness and/or a weak solid thermal conductivity, furthermore the numerical study of

Piva et al. [10] shows that the solid axial conduction tends to annihilate the level off of the Nusselt number at the pipe exit. The azimuthal temperature variation at the outer surface of an electrically and uniformly heated Inconel horizontal pipe is reported in the experimental study of Abid et al. [11]. The considered pipe is 1m long having a 1cm outer diameter and 0.02 cm thickness. The infrared thermal imaging measurements of the temperature at the pipe outer surface has shown a temperature difference between the top and bottom of the pipe that increases from 0 °C at the inlet of the pipe to 25 °C at the exit. The simultaneously developing mixed convection, with constant physical properties, in an inclined heated pipe is considered in the recent numerical study of Ouzzane and Galanis [12, 13]. In [12], the upper half pipe is heated uniformly whereas the lower half pipe is insulated. Two Grashof numbers 10^5 and 10^6 are considered for the cases of copper, steel and glass pipes. It is found that for the same Grashof number (10^5), far from the entrance, the fraction of the energy transferred to the fluid at the lower half of the pipe is 72 %, 60 % and 30 % for the copper, steel and glass pipes, respectively. This is evidence of the importance of solid conduction. In [13], the authors studied four different cases: the pipe thickness is considered or neglected and in each case the heating is over the entire circumference or over the top half of it, the lower half being insulated. It is reported that neglecting the circumferential conduction within the pipe thickness leads to an overestimation of the azimuthally wall temperature difference, at a given pipe section.

It is important to mention that in the studies of references [6-13] the fluid thermophysical properties are considered constant. However, Shome and Jensen [14] studied the mixed convection with variable viscosity in a pipe having an isothermal lateral surface. This study reported that the consideration of variable viscosity increases the average Nusselt number. In another study, Shome [15] has shown that an uncertainty of 10 % for the viscosity, thermal conductivity, density and specific heat leads to an uncertainty of the order of 5 % for the Nusselt number. It is reported that the impact of the viscosity uncertainty is the most important. The numerical study of the mixed convection, with variable physical properties, in a horizontal heated pipe without a thickness was considered by Zhang and Bell [16]. At the pipe wall, a heat flux having an imposed angular variation is supplied**.** It is reported that the imposed heat flux angular variation improves the agreement with the experimental results.

To the writers' knowledge no numerical solution is available for this combination: temperature-dependent fluid properties as well as uniform volumetric heat generation in the pipe wall with natural convection and radiation losses. This specific case is numerically simulated and the conservation equations are resolved without neglecting the axial viscous and thermal diffusion. This case is chosen to allow the comparison with the experimental results of Abid et al. [11].

2. THE GEOMETRY AND THE MATHEMATICAL MODEL

Figure 1 illustrates the problem geometry. We consider a long horizontal pipe having a length L = 1 m, an inside diameter $D_i = 0.96$cm and an external diameter $D_o = 1$cm.

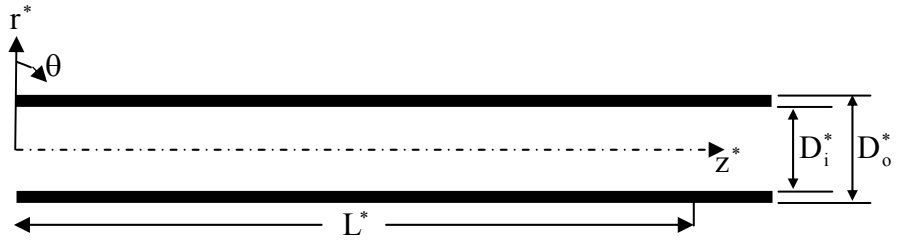

Fig. 1: Geometry and dimensions: $D_i^* = 1$, $D_o^* = 1.04$, $L^* = 104.17$

The pipe is made of Inconel having a thermal conductivity K_s = 15 W/m°K. A uniform electric internal heat generation in the entire wall thickness, equal to $4\,10^7$ W/m^3, is used to heat a laminar incompressible flow of distilled water with an average velocity equal to $1.7\,10^{-2}$ m/s. The outer surface of the pipe is not insulated and the heat losses by radiation and natural convection to the surrounding air, are taken into account. At the pipe entrance, we have a Poiseuille flow with a uniform temperature. The mentioned geometric, thermal and dynamic parameters are chosen to allow the comparison with the available experimental results of Abid et al. [11]. At the pipe exit, the axial convective fluxes of momentum are considered much greater than the diffusive ones justifying the use of null velocity gradients at the pipe exit. At the same location, the axial diffusive heat flux is assumed constant, justifying the use of a null derivative of the axial diffusive heat flux. The fluid viscosity and thermal conductivity are known functions of the temperature. The density is a linear function of temperature and the Boussinesq approximation is applied. The combined heat transfer in the solid and fluid domains is a conjugate heat transfer problem. The physical principles involved in this problem are well modeled by the following non dimensional conservation partial differential equations with their boundary conditions:

Mass conservation equation

$$\frac{1}{r^*}\frac{\partial}{\partial r^*}(r^*\,V_r^*) + \frac{1}{r^*}\frac{\partial V_\theta^*}{\partial \theta} + \frac{\partial V_z^*}{\partial z^*} = 0 \tag{1}$$

Radial momentum conservation equation

$$\begin{aligned}&\frac{\partial V_r^*}{\partial t^*} + \frac{1}{r^*}\frac{\partial}{\partial r^*}(r^* V_r^* V_r^*) + \frac{1}{r^*}\frac{\partial}{\partial \theta}(V_\theta^*\, r^*) + \frac{\partial}{\partial z^*}(V_z^* V_r^*) - \frac{V_\theta^{*2}}{r^*} = \\ &-\frac{\partial P^*}{\partial r^*} + \frac{Gr_0^*}{Re_0^2}\cos\theta\, T^* + \frac{1}{Re_0}\left[\frac{1}{r^*}\frac{\partial}{\partial r^*}(r^*\tau_{rr}^*) + \frac{1}{r^*}\frac{\partial}{\partial \theta}(\tau_{r\theta}^*) - \frac{\tau_{\theta\theta}^*}{r^*} + \frac{\partial}{\partial z^*}(\tau_{rz}^*)\right]\end{aligned} \tag{2}$$

Angular momentum conservation equation

$$\begin{aligned}&\frac{\partial V_\theta^*}{\partial t^*} + \frac{1}{r^*}\frac{\partial}{\partial r^*}(r^* V_r^* V_\theta^*) + \frac{1}{r^*}\frac{\partial}{\partial \theta}(V_\theta^* V_\theta^*) + \frac{\partial}{\partial z^*}(V_z^* V_\theta^*) + \frac{V_r^* V_\theta^*}{r^*} = \\ &-\frac{1}{r^*}\frac{\partial P^*}{\partial \theta} - \frac{\mathbf{Gr_0^*}}{\mathbf{Re_0^2}}\sin\theta\, T^* + \frac{\mathbf{1}}{\mathbf{Re_0}}\left[\frac{1}{r^{*2}}\frac{\partial}{\partial r^*}(r^{*2}\tau_{\theta r}^*) + \frac{1}{r^*}\frac{\partial}{\partial \theta}(\tau_{\theta\theta}^*) + \frac{\partial}{\partial z^*}(\tau_{\theta z}^*)\right]\end{aligned} \tag{3}$$

Axial momentum conservation equation

$$\begin{aligned}&\frac{\partial V_z^*}{\partial t^*} + \frac{1}{r^*}\frac{\partial}{\partial r^*}(r^* V_r^* V_z^*) + \frac{1}{r^*}\frac{\partial}{\partial \theta}(V_\theta^* V_z^*) + \frac{\partial}{\partial z^*}(V_z^* V_z^*) = \\ &-\frac{\partial P^*}{\partial z^*} + \frac{\mathbf{1}}{\mathbf{Re_0}}\left[\frac{1}{r^*}\frac{\partial}{\partial r^*}(r^*\tau_{rz}^*) + \frac{1}{r^*}\frac{\partial}{\partial \theta}(\tau_{\theta z}^*) + \frac{\partial}{\partial z^*}(\tau_{zz}^*)\right]\end{aligned} \tag{4}$$

Energy conservation equation

$$\frac{\partial T^*}{\partial t^*} + \frac{1}{r^*}\frac{\partial}{\partial r^*}(r^* V_r^* T^*) + \frac{1}{r^*}\frac{\partial}{\partial \theta}(V_\theta^* T^*) + \frac{\partial}{\partial z^*}(V_z^* T^*) = G^* - \frac{\mathbf{1}}{\mathbf{Re_0 Pr_0}}\left[\frac{1}{r^*}\frac{\partial}{\partial r^*}(r^* q_r^*) + \frac{1}{r^*}\frac{\partial}{\partial \theta}(q_\theta^*) + \frac{\partial}{\partial z^*}(q_z^*)\right] \tag{5}$$

where $G^* = \begin{cases} K_s^*/(Re_0\, Pr_0) & \text{in the solid} \\ 0 & \text{in the fluid} \end{cases}$

The viscous stress tensor components are:

$$\tau_{rr}^* = 2\mu^* \frac{\partial V_r^*}{\partial r^*} \qquad \tau_{r\theta}^* = \tau_{\theta r}^* = \mu^* \left[r^* \frac{\partial}{\partial r^*}\left(\frac{V_\theta^*}{r^*}\right) + \frac{1}{r^*}\frac{\partial V_r^*}{\partial \theta}\right]$$

$$\tau_{\theta\theta}^* = 2\mu^* \left[\left(\frac{1}{r^*}\frac{\partial V_\theta^*}{\partial \theta} + \frac{V_r^*}{r^*}\right)\right] \qquad \tau_{\theta z}^* = \tau_{z\theta}^* = \mu^* \left[\frac{\partial V_\theta^*}{\partial z^*} + \frac{1}{r^*}\frac{\partial V_z^*}{\partial \theta}\right] \tag{6}$$

$$\tau_{zz}^* = 2\mu^* \frac{\partial V_z^*}{\partial z^*} \qquad \tau_{zr}^* = \tau_{rz}^* = \mu^* \left[\frac{\partial V_z^*}{\partial r^*} + \frac{\partial V_r^*}{\partial z^*}\right]$$

and the heat fluxes are:

$$q_r^* = -K^* \frac{\partial T^*}{\partial r^*}\ ,\ q_\theta^* = -\frac{K^*}{r^*}\frac{\partial T^*}{\partial \theta} \text{ and } q_z^* = -K^* \frac{\partial T^*}{\partial z^*} \tag{7}$$

The boundary conditions

The previous differential equations are solved with the following boundary conditions :

At the pipe entrance: $z^* = 0$

In the fluid domain:

$$0 \le r^* \le 0.5 \text{ and } 0 \le \theta \le 2\pi : V_r^* = V_\theta^* = T^* = 0\,,\ V_z^* = 2(1 - 4r^{*2}) \tag{8}$$

In the solid domain:

$$0.5 \le r^* \le 0.5208 \text{ and } 0 \le \theta \le 2\pi : V_r^* = V_\theta^* = V_z^* = T^* = 0 \tag{9}$$

At the pipe exit: $z^* = 104.17$

In the fluid domain:

$$0 \le r^* \le 0.5 \text{ and } 0 \le \theta \le 2\pi : \frac{\partial V_r^*}{\partial z^*} = \frac{\partial V_\theta^*}{\partial z^*} = \frac{\partial V_z^*}{\partial z^*} = \frac{\partial}{\partial z^*}\left(K^* \frac{\partial T^*}{\partial z^*}\right) = 0 \tag{10}$$

In the solid domain:

$$0.5 \le r^* \le 0.5208 \text{ and } 0 \le \theta \le 2\pi : \; V_r^* = V_\theta^* = V_z^* = \frac{\partial}{\partial z^*}\left(K^* \frac{\partial T^*}{\partial z^*}\right) = 0 \tag{11}$$

At the pipe axis, the dynamical axial condition is considered.

At the pipe outer wall, the non slip condition is imposed and the radial conductive heat flux is equal to the sum of the heat fluxes of the radiation and natural convection losses.

$$r^* = 0.5208 \quad \text{for } 0 \le \theta \le 2\pi \text{ and } 0 \le z^* \le 104.17$$

$$\begin{cases} V_r^* = V_\theta^* = V_z^* = 0 \\ -K^* \dfrac{\partial T^*}{\partial r^*} = \dfrac{\left(h_r + h_c\right) D_i}{K_0} T^* \end{cases} \tag{12}$$

where:

$$h_r = \varepsilon \sigma \left(T^2 + T_\infty^2\right)\left(T + T_\infty\right) \tag{13}$$

The outer wall emissivity is $\varepsilon = 0.9$ and $\sigma = 5.67\ 10^{-8}\ W\,m^{-2}\,K^{-4}$ is the Stephan-Boltzmann constant. h_c is derived from the correlation of Churchill and Chu [17] valid for all Pr and for Rayleigh numbers in the range : $10^{-6} \le Ra \le 10^9$:

$$Nu = \left[h_c\, D_i / K_{air}\right] = \left[0.6 + \left(0.387\, Ra^{1/6} \Big/ \left(1 + (0.559/Pr_{air})^{9/16}\right)^{8/29}\right)\right]^2 \tag{14}$$

Although this correlation gives the mean Nusselt number for the whole pipe; it is approximately used to obtain the local heat transfer coefficient. The correlation is used locally with the local Rayleigh and Prandtl numbers defined as:

$$Ra = \frac{g\beta\left[T(R_o, \theta, z) - T_\infty\right] D_o^3}{\alpha_{air}\, \nu_{air}} \quad , \quad Pr_{air} = \nu_{air} / \alpha_{air} \, .$$

The air thermophysical properties are evaluated at the local film temperature:

$$T_{film} = \left[T(R_o, \theta, z) + T_\infty\right]/2$$

Along the angular direction we have the periodic conditions:

$$\text{for } 0 \le r^* \le 0.5208 \text{ and } 0 \le z^* \le 104.17 \quad \begin{cases} V_r^*(r^*, 0, z^*, t^*) = V_r^*(r^*, 2\pi, z^*, t^*) \\ V_\theta^*(r^*, 0, z^*, t^*) = V_\theta^*(r^*, 2\pi, z^*, t^*) \\ V_z^*(r^*, 0, z^*, t^*) = V_z^*(r^*, 2\pi, z^*, t^*) \\ T(r^*, 0, z^*, t^*) = T(r^*, 2\pi, z^*, t^*) \end{cases} \tag{15}$$

The Reynolds $Re_0 = 143.2836$, Grashof $Gr_0^* = 2.57534\ 10^5$ and Prandtl $Pr_0 = 8.082$ numbers are evaluated with the physical properties of water at the reference temperature ($T_0 = 288\,K$, at the pipe entrance). The non dimensional fluid viscosity and thermal conductivity variation with temperature are represented by the functions $\mu^*(T^*)$ and $K^*(T^*)$

obtained by smooth fittings of the tabulated values cited by Baehr and Stephan [18]. These functions are:

$$\mu^*(T^*) = 0.23087 + 0.78727\ \exp(-T^*/0.11386) \tag{16}$$

$$K^*(T^*) = 1.00111 + 0.80477\ T^* - 1.06002\ T^{*2} \tag{17}$$

The fittings are good approximations in the temperature range of this study. The solid non dimensional thermal conductivity is finite and constant in the temperature range of this study:

$$K_s^*(T^*) = K_s/K_0 = 25.45 \tag{18}$$

The solid non dimensional viscosity is infinite, valued to:

$$\mu_s^*(T^*) = 10^{30} \tag{19}$$

This very large viscosity within the solid domain ensures that the velocity of this part remains null. Thus, in the solid pipe thickness (the velocity is kept null), the heat transfer is only by conduction. This non-separation procedure of the solid and fluid domains is discussed in Patankar [19].

At the solid-fluid interface, the local Nusselt number is defined as:

$$Nu(\theta, z^*) = \frac{h(\theta, z)\, D_i}{K_0} = \left[\frac{(K^*\, \partial T^*/\partial r^*)\big|_{r^*=0.5}}{T^*(0.5,\ \theta,\ z^*) - T_b^*(z^*)} \right] \tag{20}$$

At a given pipe section, the bulk (mixing cup) non dimensional temperature is defined by:

$$T_b^*(z^*) = \frac{\int_0^{1/2} \int_0^{2\pi} V^*(r^*, \theta, z^*).\ T^*(r^*, \theta, z^*)\ r^*\, dr^*\, d\theta}{\int_0^{1/2} \int_0^{2\pi} V(r^*, \theta, z^*)\ r^*\, dr^*\, d\theta} \tag{21}$$

We can also define another local Nusselt number depending only on the axial coordinate z^*; but averaged over the angular coordinate θ :

$$Nu(z^*) = \frac{1}{2\pi} \int_0^{2\pi} Nu\ (\theta,\ z^*)\, d\theta \tag{22}$$

Finally, we can define an average Nusselt number for the whole solid-fluid interface :

$$Nu = \frac{1}{(2\pi)(104.17)} \int_0^{2\pi} \int_0^{104.17} Nu\ (\theta,\ z^*)\, dz^*\, d\theta \tag{23}$$

3. THE NUMERICAL METHOD

The model equations Eqs.(1)-(5) are descretized using the finite volume method, well described by Patankar [19]. At the finite volumes interfaces, the thermal conductivity and viscosity are estimated so that the correct heat flux and stress are evaluated at these interfaces. This method of correct interface physical properties is well illustrated by Patankar in [19]. The power-law discretization scheme is used in our study. The SIMPLER algorithm [19] is used to obtain the sequential solution of the discretized model equations. The line by line sweeping method (involving the use of the tri-diagonal and the tri-diagonal cyclic matrices solver) is used for the iterative solution of the systems of discretization equations.

In the r^*, θ, z^* directions, three numerical grids: 26 x 22 x42, 26 x 44 x83 and 26 x 44 x162, were tested to estimate the effect of the grid resolution on the results. In the radial direction, only 5 points are located in the small solid thickness. It is found that the last two grids give similar results (for example the relative difference between the values of the maximum of the heat flux at the interface equal to 0.1 %). The results that will be presented later are those of the 26 x 44 x162 grid. Time marching, with the time step $\Delta t^* = 10^{-3}$, is continued until the steady state is reached. The steady state is checked by the satisfaction of the global mass and energy balances as well as the leveling off of the time evolution of the hydrodynamic and thermal fields.

The accuracy of the results of our numerical code has been tested by the comparison of our results with those of other researchers. A first comparison is with the results of Ouzzane and Galanis [13] who studied the non conjugate and conjugate mixed convection heat transfer in a pipe with constant physical properties of the fluid. Some of their results concern the simultaneously developing heat transfer and fluid flow in a uniformly heated inclined pipe ($\alpha = 40^\circ$). The controlling parameters of the problem are: Re = 500, Pr = 7.0, Gr = 10^4 and 10^6, $L/D_i = 90$, $R_o/D_i = 0.583$, $K_s/K_0 = 70$. The used grid is 40x36x182 in the r^*, θ and z^* directions, respectively. We reproduced the results of the cited reference concerning the conjugate and non conjugate mixed convection. In figure 2 we illustrate the axial evolution of the circumferentially averaged Nusselt number. It is seen that there is a good agreement between our results and theirs.

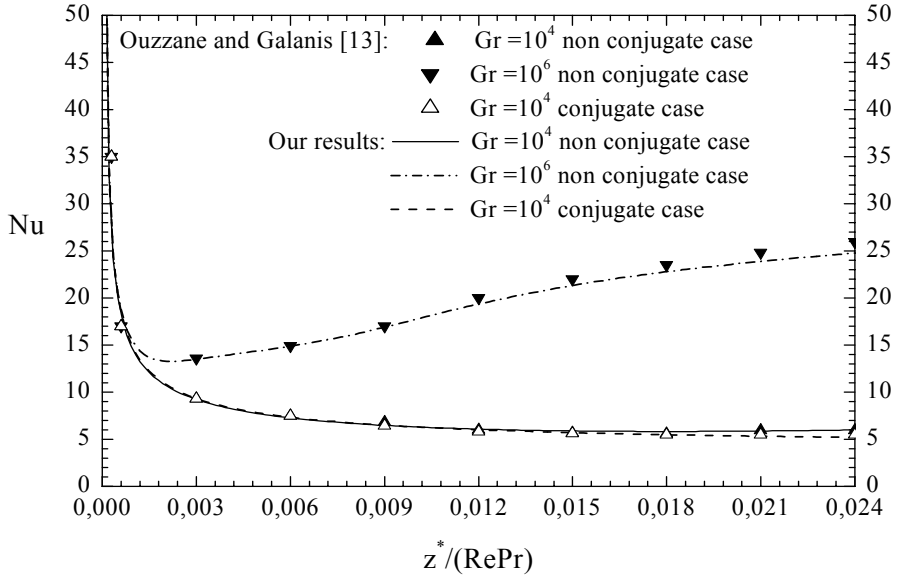

Fig. 2: Axial evolution of the circumferentially averaged Nusselt number: A reproduction of the results of Ouzzane and Galanis [13]

4. RESULTS AND DISCUSSION

4.1 The transverse fluid motion

Clearly, the fluid motion in the polar plane ($r^* - \theta$ plane) is induced by the buoyancy force that is dependent on the temperature distribution within the pipe. Moreover, this motion is influenced by the viscosity variation with temperature (to be discussed later). The formation of the transverse flow may be explained as follows. At a given pipe section, the hot fluid rises from the bottom of the pipe ($\theta = \pi$), along the hot inner wall, towards the top of the pipe ($\theta = 0$) and then descends from the top towards the bottom, in the middle of the pipe, through the core fluid. The vertical plane passing through the angles $\theta = 0$ and $\theta = \pi$ is a plane of symmetry and thus, the transverse flow, in the $r^* - \theta$ plane, is represented by two similar but counter rotating cells. This is the basic form of the transverse flow.

We remind that at the entrance, the transverse flow is inexistent. In figure 3, we show the transverse flow vector field at selected axial stations. Along the axial direction, between the entrance and $z^* = 5.53403$, the transverse flow intensifies rapidly. Along the angular direction, closer to the hot wall, the transverse flow of the right hand cell, accelerates from the bottom of the pipe ($\theta = \pi$) to an angle less than $\theta = \pi/2$.

After that, it decelerates towards the top of the pipe ($\theta = 0$). Then, it returns to the bottom of the pipe through the core fluid. At $z^* = 5.53403$, the maximum $V_\theta = 0.1272$ is located at $r^* = 0.4375$ and $\theta = 1.428$ (in the right hand cell). The centers of the rotating cells are in the upper part of the pipe, but very close to the plane dividing the upper and bottom parts of the pipe.

Between $z^* = 5.53403$ and $z^* = 36.13395$, the transverse flow decelerates because of the establishment of the stable thermal stratification zone in the upper part of the pipe. In this part, the relatively hotter fluid superposes the relatively colder fluid and this stable thermal stratification tends to inhibit the motion of the transverse flow in this zone.

This effect weakens the transverse flow in the mentioned z^* range. We noticed that the centers of the rotating cells shift downward continuously along the axial direction. At $z^* = 36.13395$, the maximum $V_\theta = 0.08253$ is located at $r^* = 0.4625$ and $\theta = 1.8564$ (in the right hand cell).

Between $z^* = 36.13395$ and $z^* = 104.17$, the shape of the transverse flow is invariant. We noticed that the form and the position of the cells of the transverse flow are invariant in this axial range. However, quantitatively, the velocity, within the two cells of the transverse flow, continues to increase slowly along the axial direction. The maximum angular velocity increases axially. At $z^* = 104.17$, the maximum $V_\theta = 0.09034$ is located at $r^* = 0.4625$ and $\theta = 1.9991$ (in the right hand cell). This axial increase of V_θ may be explained as follows.

First, in the mentioned axial range, the polar distribution of the form of the transverse flow is invariant. Second, along the pipe axial direction, the temperature rise increases the buoyancy force (the generating source of the transverse flow) and reduces the viscosity (which reduces the dissipation of the mechanical energy of the transverse flow).

Therefore, the level of the velocity of the transverse flow increases axially, although slightly. Thus, we cannot state that beyond $z^* = 36.13395$, the transverse flow is axially developed, but the form of it cells is.

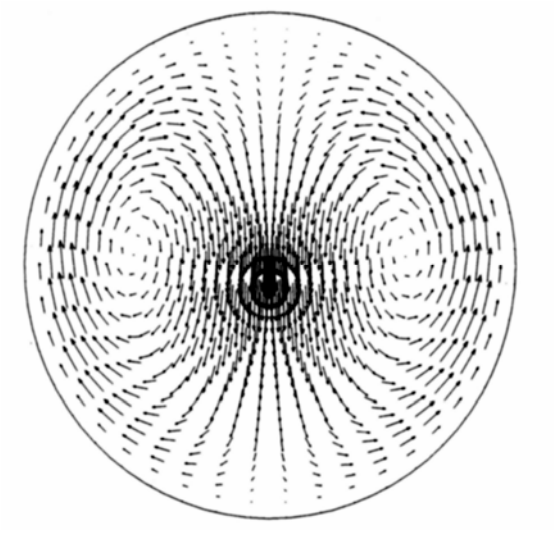

$z^* = 5.53403$

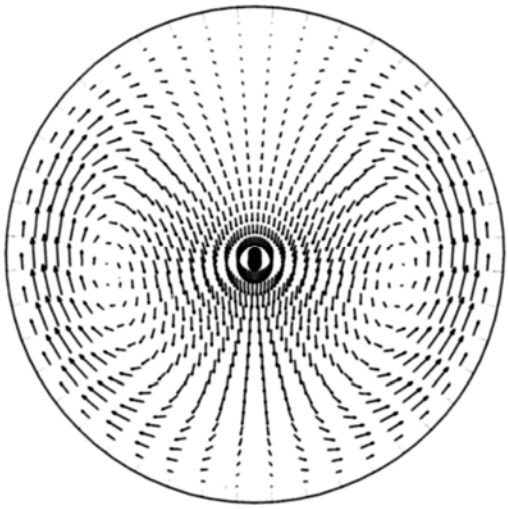

$z^* = 10.74253$

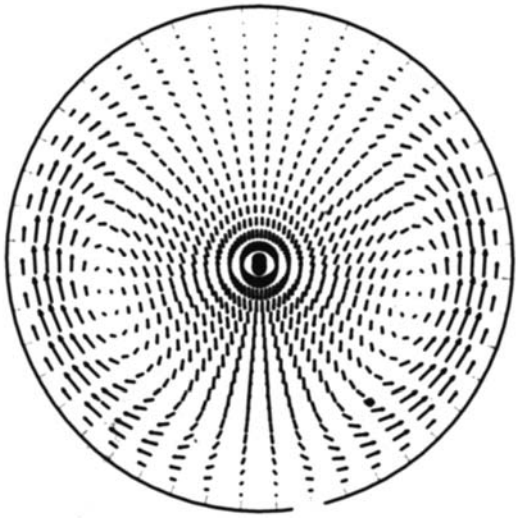

$z^* = 18.55527$

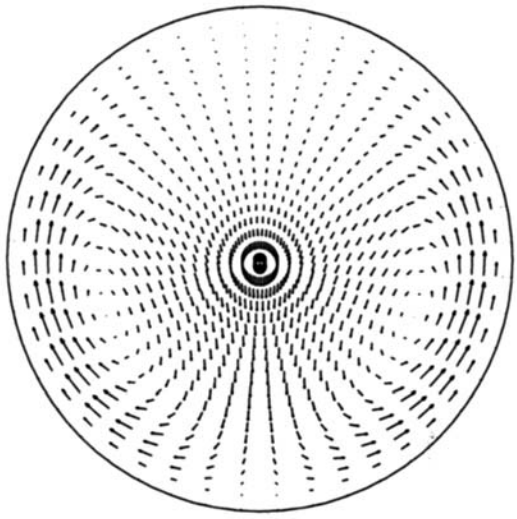

$z^* = 36.13395$

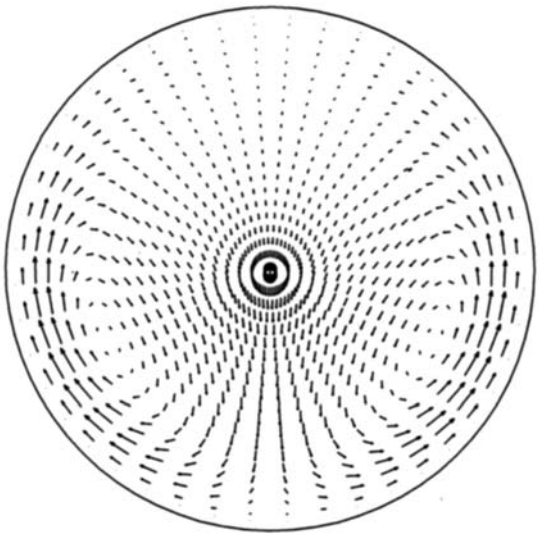

$z^* = 104.17$

Fig. 3: The polar distribution of the transverse flow at selected axial positions

4.2 The temperature field

Without the buoyancy and the variation of the viscosity and thermal conductivity effects, the temperature variation is only in the radial and axial direction. In this case, the temperature distribution is well described by the classic axisymmetric forced convection thermal field. The temperature increases axially and at any pipe section (fixed z^*), the isotherms are concentric circles with the maximum temperature located on the pipe wall and the minimum temperature located on the pipe axis. As mentioned before, the mixed convection induces a transverse flow that imparts to the temperature field an angular variation within the fluid domain and the pipe solid thickness. The hot fluid closer to the pipe wall is driven (by the transverse flow) upward towards the top of the pipe, and then, is circulated downward towards the bottom of the pipe, passing through the relatively colder core fluid. This must establish a stable thermal stratification zone in the region between the upper part of the pipe and the colder core fluid.

The size of this zone is expected to increase axially as the coldest core is expected to be continuously driven downward (by the transverse flow). This qualitative temperature distribution within the fluid leads to some expectation concerning the temperature variation on the pipe inner wall ($r^* = 0.5$), separating the solid and fluid domains. It is expected that, downstream from the entrance, at any pipe section, at the solid-fluid interface, the maximum temperature will be at $\theta = 0$ and the minimum temperature at $\theta = \pi$. This angular temperature variation, along the pipe inner wall, is expected to cause an angular variation of the radial heat flux from the solid to the fluid (as it will be shown later). This angular variation of the radial heat flux undoubtedly influences the level of the temperature angular variation itself. Moreover, the level of temperature must increase axially because of the continuous heat input. This discussion reveals the physically sound and acceptable temperature qualitative axial and angular variations within the fluid and at the solid-fluid interface. The quantitative variation of the thermal field is determined by the values of the controlling parameters of the conjugate heat transfer problem. The temperature variation in the physical domain is dependent on the convection and conduction within the fluid domain and the conduction within the solid wall, which are dependent. This is the conjugate heat transfer problem at hand. The conduction within the solid depends on the heat generation, the wall thickness, the solid thermal conductivity, the fluid convective effect on the solid-fluid interface and the minor heat losses (they are minor indeed in our case) from the pipe outer wall to the atmosphere. The heat transfer in the fluid domain depends on the radial heat flux from the solid to the fluid at their interface, the flow field and the variation of the physical properties with temperature.

To illustrate the obtained thermal field, we show in figure 4, the polar temperature distribution at selected axial positions. Away from the entrance, at a given pipe section, the convective motion of the transverse flow flattens the isotherms between the upper part of the pipe and colder core fluid. In this part, the temperature distribution is according to the stable thermal stratification: the temperature decreases from the top of the pipe towards the colder core fluid. Also, as expected, there is a continuous axial increase of the level of temperature. We notice that there is negligible temperature radial variation within the small solid thickness due to its negligible thermal resistance. Away from the entrance, for a given pipe section, the maximum temperature is at the top of the pipe. The minimum temperature is within the core fluid, in the lower part of the pipe at $\theta = \pi$. Along the axial direction, the radial position of the minimum temperature is driven downward from the pipe axis, and this is the expected effect of the convective transverse flow. At $z^* = 5.53403$, the position of the minimum sectional temperature is located at $r^* = 0.2625$. This position shifts to $r^* = 0.3125$,

$r^* = 0.3375$, $r^* = 0.3375$ and $r^* = 0.3625$, at $z^* = 10.74253$, $z^* = 18.55527$, $z^* = 36.13395$, and $z^* = 104.17$, respectively. We observe that the obtained thermal field is physically sound and acceptable.

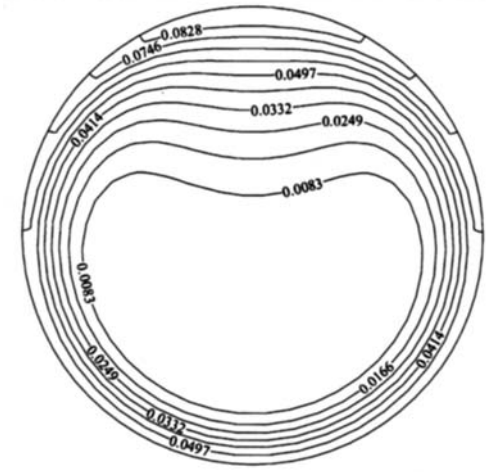

$z^* = 5.53403$

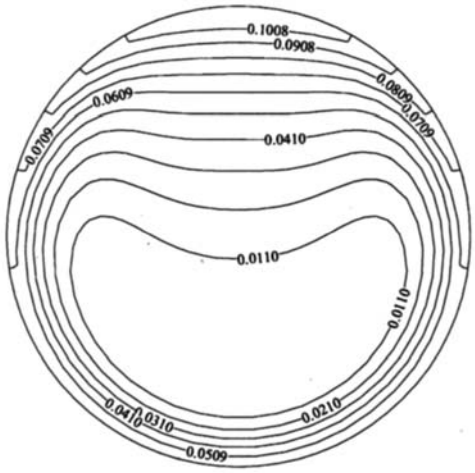

$z^* = 10.74253$

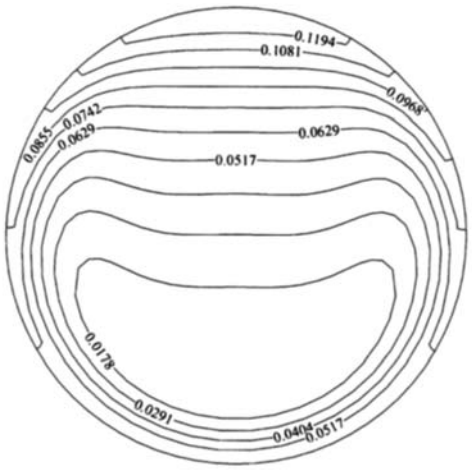

$z^* = 18.55527$

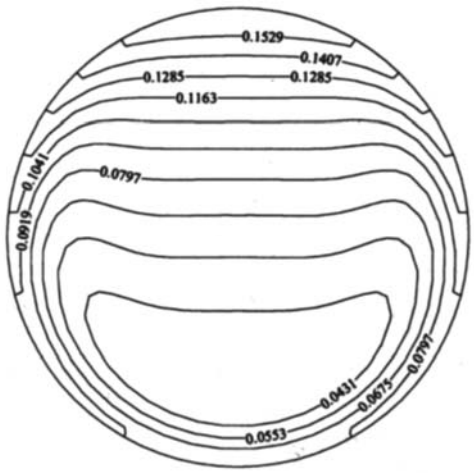

$z^* = 36.13395$

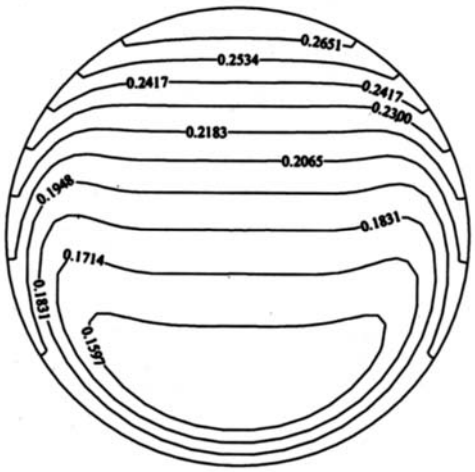

$z^* = 104.17$

Fig. 4: The polar distribution of the temperature field at selected axial positions

In figure 5, we compare our numerical result with the experimental result of Abid et al. [11]. In this figure we present the axial variation of the temperature at $r^* = 0.5208$ and $\theta = 0$ (top of the outer wall of the pipe) and the temperature at $r^* = 0.5208$ and $\theta=\pi$ (bottom of the outer wall of the pipe). The temperature and axial position are presented in dimensional form as in the experimental reference. In the experiment the temperature was measured by infra-red imaging. It is seen in the figure that we have a good agreement with the experimental results. This agreement validates the level and the axial and angular variations of the obtained numerical thermal field.

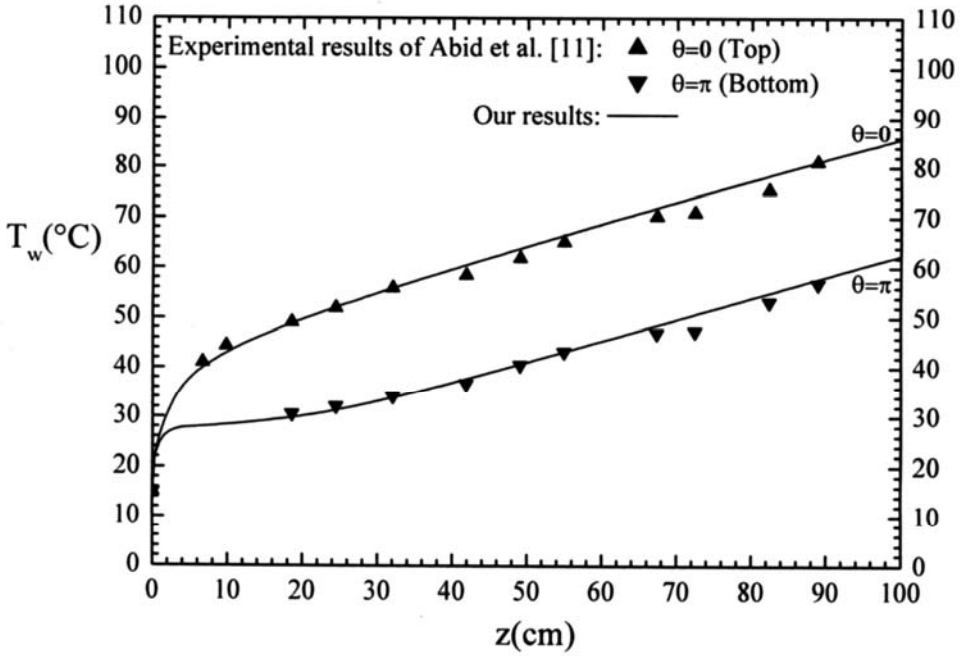

Fig. 5: Axial variation of the outer wall temperature:
A comparison with the experimental results of Abid et al. [11]

4.3 The radial non dimensional heat flux at the solid-fluid interface

This is the radial heat flux delivered to the fluid domain at the solid-fluid interface. Although the heat generation within the pipe thickness is constant, the inner radial heat flux at the solid-fluid interface (defined as $K^* \dfrac{\partial T^*}{\partial r^*}$ at $r^* = 0.5$) has axial and angular variations. The radial inner heat flux angular variation is caused mainly by the angular temperature variation at the solid-fluid interface and to a very small degree by the asymmetry of the heat losses to the ambient air. We found that these losses are small: the global heat losses are 6.55 % of the generated heat; valued to 6 % in the experiment of Abid et al. [11]. Most of the generated heat is transferred to the flowing water. The angular variation of the inner heat flux is illustrated in figure 6, at selected axial positions. Very close to the entrance (at $z^* = 0.3255$), the buoyancy effect (and thus the angular temperature variation) is very weak and the heat flux has no angular variation. Away from the entrance, at a given section, the interface radial heat flux increases between $\theta = 0$ and an angle equal to or less than $\theta = \pi/2$ (depending on the axial position). Between this angle and $\theta = \pi$, the heat flux decreases. However, the heat flux at $\theta = \pi$ is higher than that $\theta = 0$. By symmetry, from $\theta = 2\pi$ to $\theta = \pi$, the angular distribution of the inner heat flux is the same as that between $\theta = 0$ and $\theta = \pi$.

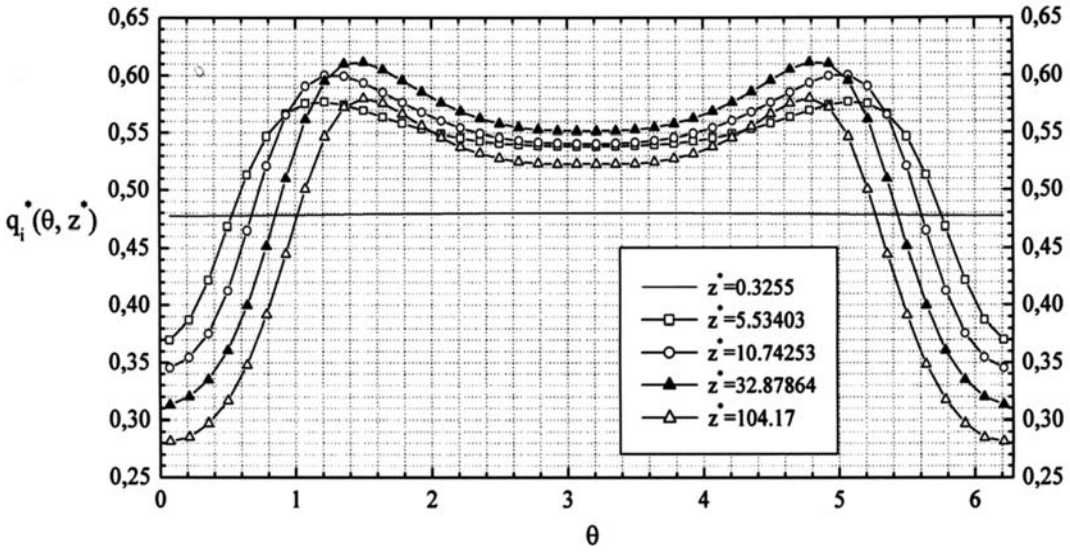

Fig. 6: Variation of the local heat flux at the solid-fluid interface

The qualitative angular variation of the interface heat flux is compatible with that of the transverse flow closer to the interface. We mentioned before that, closer to the wall, the transverse flow accelerates from the bottom of the wall to a maximum strength around $\theta = \pi/2$ (in the right hand cell) and then decelerates towards the top of the pipe. The interface radial heat flux is proportional to the nearby velocity of the transverse flow. That is to say, the convective heat transfer of the transverse flow (proportional to its velocity closer to the wall) must be compensated by a proportional radial heat flux, at the interface, to keep the required level of the local temperature. Within a pipe section, where the strength of the transverse flow is higher the interface radial heat flux is higher and vice versa.

Clearly, the conjugate heat transfer at hand is not the case of a constant heat flux (into the fluid) imposed at the solid-fluid interface; although the heat generation within the small solid pipe thickness is uniform. The considerable angular variation of the radial heat flux at the interface justifies the properly used conjugate heat transfer model.

4.4 The local and averaged Nusselt numbers

The axial and angular variations of the interface local Nusselt number is shown in figure 7. This Nusselt number is defined in Eq. (20). From the entrance to $z^* = 0.97659$, there is an axial drop of the local Nusselt number and a negligible angular variation. In this region, the distribution of the local Nusselt number is similar to that of a thermally developing forced convection regime. From $z^* = 0.97659$ to the exit, we noticed large axial and angular variations. There is a monotonic axial increase of the local Nusselt number which is characteristic of the enhanced heat transfer by the continuous mixing effect of the transverse flow. At a given pipe section, the minimum local Nusselt number is at $\theta = 0$ and the maximum local Nusselt number is at $\theta = \pi$. Between these angular positions, the local Nusselt number increases monotonically and significantly. By symmetry, from $\theta = 2\pi$ to $\theta = \pi$, the angular distribution of the local Nusselt number is the same as that between $\theta = 0$ and $\theta = \pi$. The angular variation of the local Nusselt number is, by definition, determined by the angular variation of the radial heat flux at the interface (discussed before) and the angular variation of the difference of the local interface temperature and the mixing cup temperature.

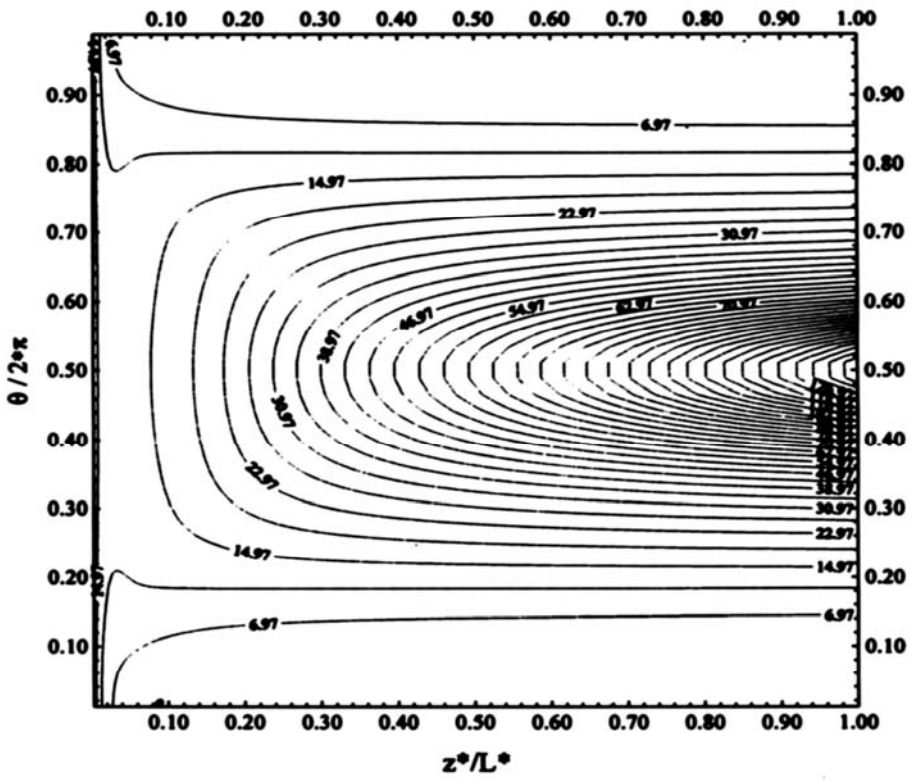

Fig. 7: Distribution of the local Nusselt number Nu (θ, z^*) at the interface

At a given pipe section, the mixing cup temperature is constant and thus the temperature difference increases monotonically and significantly from the bottom ($\theta = \pi$) to the top of the pipe ($\theta = 0$). It is this variation of the temperature difference that gives to the local Nusselt number its qualitative increase from the bottom to the top of the pipe. The angular variation of the interface radial heat flux affects only, locally, the level of the increase. As an example, at $z^* = 32.879$, we show in figure 8 the angular variation of the interface radial heat flux, the temperature difference and their ratio: the local Nusselt number (normalized by its maximum value at $\theta = \pi$ for a good graphical presentation).

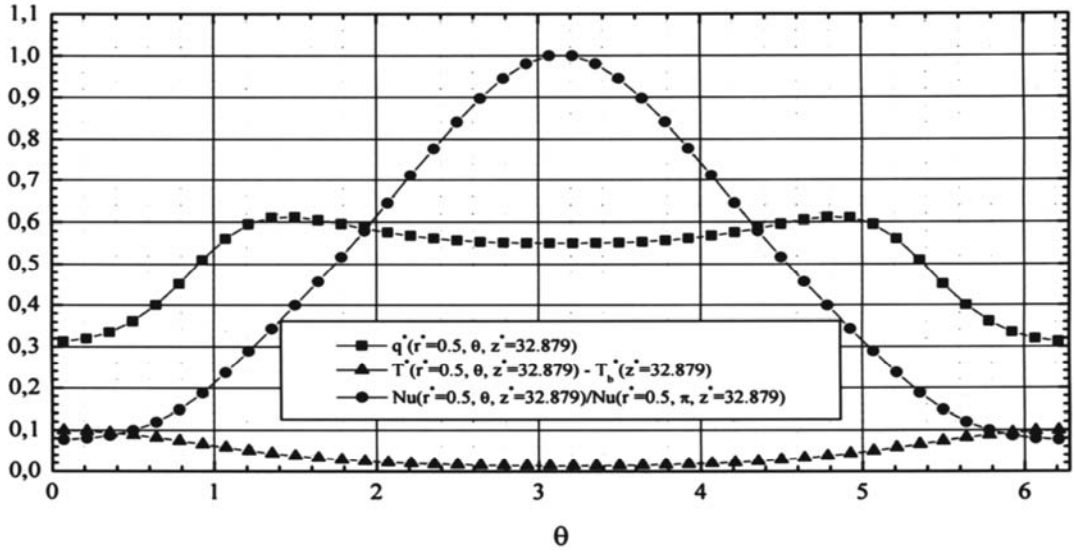

Fig. 8: Interface radial heat flux, temperature difference and Nusselt number at $z^* = 32.879$

If we average the local Nusselt number over the angular direction, we obtain the axial variation of the interface Nusselt number as defined in Eq. (22). The axial variation of the Nusselt number is shown in figure 9. Also, we have calculated and reported in this figure the classical case corresponding to the pure forced convection ($Gr^* = 0$). It is seen that the mixed convection Nusselt number decreases from 17.692 at the entrance to 10.571 at $z^* = 4.23191$ following the forced convection case, and from this position to the pipe exit, it detaches and increases monotonically due to the enhanced heat transfer by the transverse flow. The axial increase is characteristic of the mixed convection heat transfer. At the pipe exit, the axial Nusselt number is equal to 39.69. If we average the local Nusselt number over the axial and angular directions, as defined by Eq. (23), we obtain the average Nusselt number for the whole pipe inner wall. This average Nusselt number is equal to 24.808.

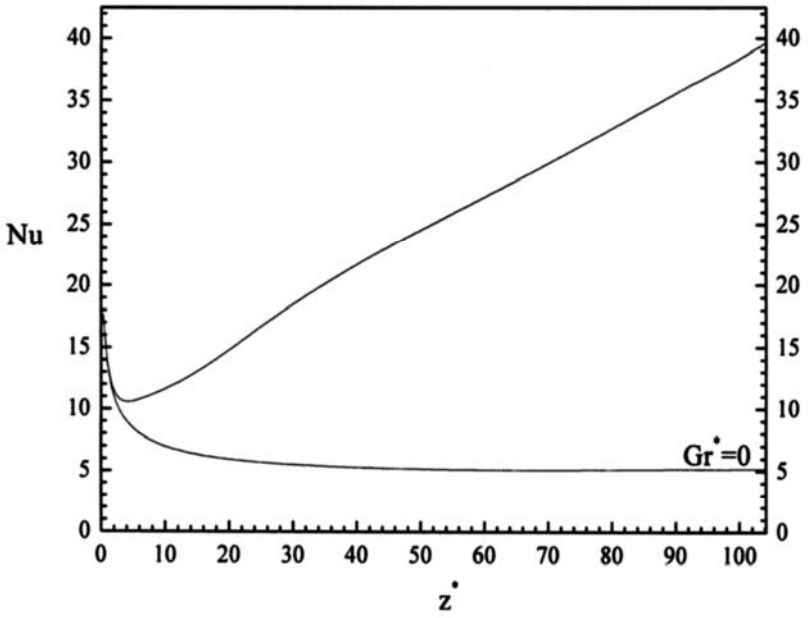

Fig. 9: Axial evolution of the circumferentially averaged Nusselt number

4.5 The fluid viscosity and thermal conductivity distributions

From the entrance to the exit of the pipe we find a significant variation of viscosity. The maximum viscosity is at the pipe entrance ($\mu^* = 1$) and the minimum one ($\mu^* = 0.302104$), is located at the top of the inner wall, at the exit of the pipe. It is seen that the viscosity decreases downstream and at a given pipe section, the viscosity is lower closer to the pipe wall and increases towards the relatively cold core fluid. It is also clear that, closer to the wall, along the angular direction, the viscosity decreases continuously from the top to the bottom of the pipe.

However, there is a relatively small angular and axial variations of the thermal conductivity from the entrance to the exit of the pipe. The minimum is at the pipe entrance ($K^* = 1$) and the maximum one ($K^* = 1.14193$), is located at the top of the inner wall, at the exit of the pipe.

For the sake of brevity, the shape of these distributions that to follow qualitatively the shape of the temperature field are not reported.

5. CONCLUSION

This study considers the numerical simulation of the heat transfer and fluid flow in a horizontal pipe having a small thickness within which there is uniform heat generation. It has shown that the realistic consideration of the three dimensional conjugate heat transfer (conduction in the solid and mixed convection in the fluid), with variable physical properties, properly models the problem and reproduces the experimental results with a good accuracy. The obtained flow field is three directional (with three velocity components) and three dimensional (depending on the three cylindrical coordinates). The heat transfer is considerably enhanced by the mixing effect of the transverse flow. Although the heat generation within the pipe thickness is uniform, the radial heat flux from the solid to the fluid, at their interface, has significant axial and angular variations. The conduction within the pipe thickness must be taken into account for a proper modeling of the heat input from the solid wall to the fluid. In the obtained temperature range, the variation of the fluid thermal conductivity is small but that of the viscosity is large and must also be taken into account.

Acknowledgments:

- The used 3-D Fortran code is a modified version of a constant properties code generously given to Dr. M. Afrid by Dr. A. Zebib of the Mechanical and Aerospace Engineering Department of Rutgers University, New-Jersey, U.S.A.
- This study was financially supported by the Algerian M.E.S.R.S. through the grant of the projects identified as D2501/04/97 and D2501/01/2000.
- One part of the bibliographic support was provided to T. Boufendi by Prof. F. Papini and Dr. C. Abid, I.U.S.T.I., CNRS UMR 139, Université de Provence, Technopôle Château Gombert, Marseille, France.

NOMENCLATURE

D : pipe diameter, m

g : gravitational acceleration, $(= 9.81\,m/s^2)$

Gr^* : modified Grashof number $(= g\,\beta G D_i^5 / K_s \nu^2)$

G : volumetric heat generation, W/m^3

G^* : nondimensional volumetric heat generation, $(= K_s^* / Re_0\, Pr_0)$

$h(\theta, z)$: local heat transfer coefficient, $W/m^2.K$

h_c : convective heat transfer coefficient (pipe-ambient air), $W/m^2.K$

h_r : radiative heat transfer coefficient (pipe-ambient air), $W/m^2.K$

K : fluid thermal conductivity, $W/m^2.K$

T_b^* : nondimensional mixing temperature, $(=(T_b - T_0)/(G D_i^2/K_s))$

V_0 : mean axial velocity at the pipe entrance, m/s

V_r : radial velocity component, m/s

V_r^* : nondimensional radial velocity component, $(= V_r / V_0)$

V_θ : circumferential velocity component, m/s

V_θ^* : nondimensional circumferential velocity component, $(= V_\theta / V_0)$

V_z : axial velocity component, m/s

V_z^* : nondimensional axial velocity component, $(= V_z / V_0)$

z : axial coordinate, m

K^* : non dimensional thermal conductivity, $(= K/K_0)$

K_s^* : non dimensional solid thermal conductivity, $(= K_s/K_0)$

L : pipe length, m

$Nu(\theta, z$: local Nusselt number, $(= h(\theta, z) D_i / K_0)$

$Nu(z^*)$: peripherally averaged local axial Nusselt number, $(= h(z) D_i / K_0)$

P : pressure, N/m^2

P^* : nondimensional pressure, $(= (P - P_0)/\rho_0 V_0^2)$

Pr : Prandtl number, $(= \nu/\alpha)$

q : heat flux, W/m^2

r : radial coordinate, m

r^* : nondimensional radial coordinate, $(= r / D_i)$

R : pipe radius, m

Re : Reynolds number, $(= V_0 D_i / \nu_0)$

t : time, s

t^* : nondimensional time, $(= V_0 t / D_i)$

T : temperature, K

T^* : nondimensional temperature, $(= (T - T_0)/(G D_i^2/K_s))$

T_b : mixing cup section temperature, K

z^* : nondimensional axial coordinate, $(= z / D_i)$

Greek symbols

α : thermal diffusivity, m^2/s

β : thermal expansion coefficient, $1/K$

μ : dynamic viscosity, kg·m/s

μ^* : nondimensinal dynamic viscosity, $(=\mu/\mu_0)$

ν : kinematic viscosity, m²/s

θ : angular coordinate, rad

ρ : density, kg/m^3

τ : stress, N/m^2

τ^* : non dimensional stress, $(= \tau/(\mu_0 V_0 / D_i))$

Subscripts

B : bulk

I, o : reference to the inner, outer walls of the pipe

r,θ,z : reference to the radial, tangential and axial directions respectively

∞ : reference to the ambient air away from the outer wall

0 : at pipe entrance

Superscript

$*$: Nondimensional

REFERENCES

[1] A.E. Bergles, '*Prediction of the Effect of Temperature-Dependent Fluid Properties on Laminar Heat Transfer*', in S. Kakaç, R.K. Shah and A.E. Bergles (eds.), Low Reynolds Number Flow Heat Exchangers, pp. 451-471, Hemisphere, Washington, D.C., 1983.

[2] A.E. Bergles, '*Experimental Verification of Analyses and Correlations of the Effects of Temperature-Dependent Fluid Properties on Laminar Heat Transfer*', in S. Kakaç, R.K. Shah and A.E. Bergles (eds.), Low Reynolds Number Flow Heat Exchangers, pp. 473-486, Hemisphere, Washington, D.C., 1983.

[3] W. Aung, '*Mixed Convection in Internal Flow*', in S. Kakaç, R.K. Shah and W. Aung (eds.), Handbook of Single-Phase Convective Heat Transfer, pp. 15.1-15.51, Wiley, New-York, 1987.

[4] S. Kakaç, '*The Effect of Temperature-Dependent Fluid Properties on Convective Heat Transfer*', in S. Kakaç, R.K. Shah and W. Aung (eds.), Handbook of Single-Phase Convective Heat Transfer, pp. 18.1-18.56, Wiley, New-York, 1987.

[5] A.F. Polyakov, '*Mixed Convection in Single-Phase Flows*', in O.G. Martynenko and A.A. Zukauskas (eds.), Heat Transfer: Soviet Reviews, Convective Heat Transfer, Vol.1, pp. 1-95, Hemisphere, Washington, D.C., 1989.

[6] S.M. Morcos and A.E. Bergles, '*Experimental Investigation of Combined Forced and Free Laminar Convection in Horizontal Tubes*', Trans. ASME J. Heat Transfer, Vol. 97, pp. 212-219, 1975.

[7] P.H. Newell Jr. and A.E. Bergles, '*Analysis of Combined Free and Forced Convection for Fully Developed Laminar Flow in Horizontal Tubes*', Trans. ASME J. Heat Transfer, Vol. 92, pp. 83-93, 1970.

[8] R.S. Chen and G.J. Hwang, '*Effect of Wall Conduction on Combined Free and Forced Laminar Convection in Horizontal Tubes*', Trans. ASME J. Heat Transfer, Vol. 111, pp. 581-585, 1989.

[9] J.W. Baughn, '*Effect of Circumferential Wall Heat Conduction on Boundary Conditions for Heat Transfer in a Circular Tube*', Trans. ASME J. Heat Transfer, Vol. 100, pp.537-539, 1978.

[10] S. Piva, G.S. Barozzi and W.M. Collins, '*Combined Convection and Wall Conduction Effects in Laminar Pipe Flow: Numerical and Experimental Validation under Uniform Wall Heating*', Heat Mass Transfer, Vol. 30, pp. 401-409, 1995.

[11] C. Abid, F. Papini, A. Ropke et D. Veyret, '*Etude de la Convection Mixte dans un Conduit Cylindrique. Approche Analytique/Numérique et Détermination Expérimentale de la Température de Paroi par Thermographie Infrarouge*', Int. J. Heat Mass Transfer, Vol. 37, pp. 91-101, 1994.

[12] M. Ouzzane and N. Galanis, '*Developing Mixed Convection in an Inclined Tube with Circumferentially Nonuniform Heating at its Outer Surface*', Numerical Heat Transfer, Part A, Vol. 35, pp. 609-628, 1999.

[13] M. Ouzzane et N. Galanis, '*Effets de la Conduction Pariétale et de la Répartition du Flux Thermique sur la Convection Mixte près de l'Entrée d'une Conduite Inclinée*', Int. J. Thermal Sciences, Vol. 38, pp. 622-633, 1999.

[14] B. Shome and M. K. Jensen, '*Mixed Convection Laminar Flow and Heat Transfer of Liquids in Isothermal Horizontal Circular Ducts*', Int. J. Heat Mass Transfer, Vol. 38, pp. 1945-1956, 1995.

[15] B. Shome, '*Effect of Uncertainties in Fluid Properties on Mixed Convection Laminar Flow and Heat Transfer in a Uniformly Heated Smooth Tube*', Numerical Heat Transfer, Part A, Vol. 35, pp. 875-889, 1999.

[16] C. Zhang and K. J. Bell, '*Mixed Convection in Horizontal Tubes with Nominally Uniform Heat Flux*', AIChE Symp. Ser., Vol. 88, N° 288, pp. 212-219, 1992.

[17] S.W. Churchill and H.S. Chu, '*Correlating Equation for Laminar and Turbulent Free Convection from a Horizontal Cylinder*', Int. J. Heat Mass Transfer, Vol. 18, pp. 1049-1053, 1975.

[18] H.D. Baehr and K. Stephan, '*Heat and Mass Transfer, Transl*', by N. JanePark, p. 619, Springer-Verlag, Berlin, 1998.

[19] S.V. Patankar, '*Numerical Heat Transfer and Fluid Flow*', McGraw-Hill, New-York, 1980.